JPEDAV (2006) 27:605-613
DOI: 10.1361/154770306X153620
1547-7037/$19.00 ©ASM International

Interdiffusion Kinetics in the Mo_5SiB_2 (T_2) Phase

Sungtae Kim and John H. Perepezko

(Submitted April 6, 2006; in revised form August 17, 2006)

Diffusion couples based on Mo_2B and Mo_5Si_3 were used to determine the diffusion kinetics of T_2 phase development and the relative diffusivities controlling the kinetics. Annealing the Mo_2B/Mo_5Si_3 diffusion couple above 1600 °C yielded an initial diffusion path sequence of $Mo_2B/T_2/Mo_3Si/Mo_5Si_3$, which was subsequently transformed to $Mo_2B/T_2/(Mo_3Si + Mo_5Si_3)/Mo_5Si_3$ by shrinkage of the Mo_3Si phase upon long-term annealing. The T_2 phase developed from Mo_2B and during the growth of the T_2 phase, Si and B atom movements were driven by the Si concentration gradient. The activation energy for Si interdiffusion in the T_2 phase was evaluated to be 355 kJ/mole compared with about 300 kJ/mole for Mo_5Si_3 in both Mo/Si and $MoSi_2/T_2$ diffusion couples. The larger activation energy is mainly responsible for the 10^3 lower diffusivity for Si in the T_2 phase compared with Mo_5Si_3. The relatively slow diffusion in the T_2 phase is consistent with the enhanced creep resistance exhibited by T_2 phase microstructures.

Keywords activation energy, diffusion path, interdiffusion coefficient, intermetallic compound, Mo_5SiB_2

1. Introduction

The high melting temperature and oxidation resistance of the Mo_5SiB_2 (T_2) phase and multiphase microstructures incorporating the T_2 phase in the Mo-Si-B system are attractive for applications in very high temperature environments. An essential requirement of materials for high-temperature structural applications is the maintenance of microstructure. While there are certain microstructure designs that offer the most robust performance, it is evident that the endurance of any design is determined, to a large extent, by the magnitude and rate of diffusion-induced modifications. Accordingly, the determination and analysis of diffusion kinetics is of central importance in evaluating the structural stability of multiphase microstructures.

Electron probe microanalysis (EPMA) and x-ray diffraction (XRD) examinations of as-cast and rapidly solidified samples annealed for extended times have been applied to determine the phase stability of the Mo-rich Mo-Si-B system between 1600 and 1950 °C.[1] Figure 1 shows the Mo-MoB-Mo_5Si_3 region of the phase diagram (excluding the two-phase equilibrium region of MoB-Mo_5Si_3) at 1600 °C, where the boundary lines are plotted on the basis of composition data for phases obtained using EPMA. The T_2 phase shows an appreciable compositional homogeneity range around the stoichiometric composition and is in equilibrium with Mo_{ss}, Mo_2B, MoB, Mo_3Si, and Mo_5Si_3.

Direct synthesis of the T_2 phase as a single phase from the melt is possible for certain compositions,[2] but this type of sample offers limited opportunities to examine interdiffusion behavior. The T_2 phase does exhibit a stable equilibrium with a Mo solid solution, Mo(ss), as indicated in the isothermal section in Fig. 1, but there is no stable two-phase field between the T_2 phase and either B or Si. Instead, an effective sample design can be examined based on the synthesis of the T_2 phase as a reactive diffusion product between binary intermediate phase end members of a diffusion couple such as Mo_2B and Mo_5Si_3, as illustrated in Fig. 1.

The reactive silicide formation and interdiffusion in solid-solid diffusion couples that are assembled with molybdenum and molybdenum silicide have been studied extensively.[3-7] In addition, Brandstötter et al.[8] observed the formation of MoB and Mo_2B from an annealed Mo-B couple that was followed by pack boriding of Mo. Recently, Hayashi et al.[9] evaluated the growth rate constants and interdiffusion coefficients of Mo_5Si_3 and Mo_5Si_3 + MoB layers that developed within the $MoSi_2/Mo_5SiB_2$ couples. The growth for both the Mo_5Si_3 and Mo_5Si_3 + MoB layers was parabolic with annealing time, and the growth rate constants were approximately equal to each other with a value of 1.3×10^{-9} cm^2/s at 1600 °C. The average interdiffusion coefficient for Mo_5Si_3 formed in the $MoSi_2/Mo_5SiB_2$ diffusion couples was 4.1×10^{-9} cm^2/s at 1600 °C, and the activation energy for interdiffusion in Mo_5Si_3 was determined to be about 300 kJ/mol. Ito et al.[10] examined the evolution kinetics of Mo_5Si_3 in a $MoSi_2$/Mo(ss) + Mo_5SiB_2 diffusion couple. The average interdiffusion coefficient at 1500 °C was 1.2×10^{-9} cm^2/s and the activation energy for interdiffusion in Mo_5Si_3 was estimated at 240 kJ/mol. Aside from a preliminary report by Kim et al.[11] on the interdiffusion in the T_2 phase synthesized in Mo_2B/Mo_5Si_3 diffu-

This article was presented at the Multicomponent-Multiphase Diffusion Symposium in Honor of Mysore A. Dayananda, which was held during TMS 2006, 135th Annual Meeting and Exhibition, March 12-16, 2006, in San Antonio, TX. The symposium was organized by Yongho Sohn of University of Central Florida, Carelyn E. Campbell of National Institute of Standards and Technology, Richard D. Sisson, Jr., of Worcester Polytechnic Institute, and John E. Morral of Ohio State University.

Sungtae Kim and **John H. Perepezko,** Department of Materials Science and Engineering University of Wisconsin—Madison, 1509 University Ave., Madison, WI 53706. Contact e-mail: perepezk@engr.wisc.edu.

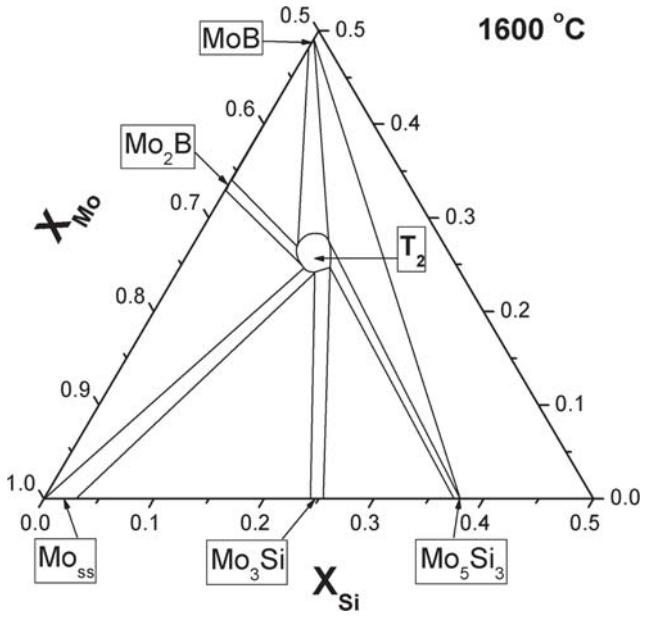

Fig. 1 Ternary isotherm at 1600 °C of the Mo-rich Mo-Si-B system. Source: Ref 1

sion couples at 1600 °C, there have been no detailed studies of the diffusion kinetics in the T_2 phase. In the current work, the relative diffusivities and related diffusion kinetics of the product T_2 phase are evaluated between 1600 and 1800 °C from diffusion couples between binary boride and silicide phases.

2. Experimental Methods

Mo_2B and Mo_5Si_3 alloys were prepared by repetitive arc melting of pure Mo and B, and pure Mo and Si in an atmosphere of high-purity (oxygen gettered) argon and homogenized at 1600 °C for 150 h. To obtain smooth surfaces, ingots were sectioned into 2 to 3 mm thick slices, ground with Al_2O_3 powder (<5 μm), and then rinsed with methyl alcohol in an ultrasonic cleaner and dried. A diffusion couple was assembled from Mo_2B and Mo_5Si_3 slices and wrapped with a Ta foil. The diffusion couples were annealed at 1600 °C under an argon atmosphere, and at 1700 and 1800 °C under high vacuum (10^{-3} to 10^{-5} Pa), respectively. The diffusion couples were cut perpendicular to the interface using a diamond-impregnated low-speed saw. Using an electron probe microanalysis (CAMECA SX50 EPMA, University of Wisconsin, Madison, WI), the compositions of diffusion couple sections were line scanned. EPMA analysis was carried out on the uncoated specimens at 7 kV and a beam current of 30 nA. This resulted in decreased electron penetration and x-ray generation closer to the surface, requiring a smaller absorption correction in the matrix correction. A serious interference problem of the first-order Mo Mζ (Mz) line with the first order B Kα line was solved by a "Probe for Window" software.[12]

3. Results and Discussion

3.1 Reactive Phase Formation in a Mo_2B/Mo_5Si_3 Diffusion Couple

Annealing the Mo_2B/Mo_5Si_3 diffusion couple resulted in the initial formation of the T_2 and Mo_3Si phases between Mo_2B and Mo_5Si_3 to develop the $Mo_2B/T_2/Mo_3Si/Mo_5Si_3$ (Fig. 2) diffusion pathway. To interpret the formation of T_2 and Mo_3Si by a thermally activated reaction between Mo_2B and Mo_5Si_3, an estimate of the driving force for nucleation can provide useful insight. In the Mo-Si-B ternary phase diagram (Fig. 1), the stable phases at 1600 °C are Mo, Mo_2B, MoB, Mo_3Si, Mo_5Si_3, and T_2, where the free energies of formation of phases excluding T_2 were calculated from the published thermodynamic property data.[13] Considering binary phases as line compounds, the unknown free energy of formation of T_2 was initially estimated by comparing the stability of each two-phase equilibrium field around the T_2 phase.

When determining the stability of a two-phase equilibrium field in a ternary system, the free energy of a set of selected two phases is compared with another set of selected two phases, where the two two-phase equilibrium fields cross each other. For instance, whether at 1600 °C the Mo_2B-Mo_5Si_3 two-phase field is more stable than the Mo-T_2 two-phase field is determined by calculating the free-energy change (ΔG^r) of a reaction: $6Mo_2B + Mo_5Si_3 \leftrightarrow 2Mo + 3T_2$. When ΔG^r ($= 2\Delta G^o_{Mo} + 3\Delta G^o_{T_2} - 6\Delta G^o_{Mo_2B} - \Delta G^o_{Mo_5Si_3}$) < 0, the Mo-T_2 two-phase field is more stable than the Mo_2B-Mo_5Si_3 two-phase field. When $\Delta G^r > 0$, the Mo_2B-Mo_5Si_3 two-phase field is more stable than the Mo-T_2 two-phase field. When $\Delta G^r = 0$, the invariant Mo-T_2-Mo_2B-Mo_5Si_3 four-phase equilibrium occurs. The existence of the stable Mo-T_2 two-phase equilibrium in Fig. 1 indicates that $\Delta G^r < 0$, and consequently the free energy of formation of T_2 satisfies $\Delta G^o_{T_2} < (⅓)(-2\,\Delta G^o_{Mo} + 6\,\Delta G^o_{Mo_2B} + \Delta G^o_{Mo_5Si_3})$, resulting in $\Delta G^o_{T_2} < -129$ kJ/g-atom ($= -1033$ kJ/1 mol of T_2). In other words, at 1600 °C the Mo-T_2 two-phase equilibrium is more stable than the Mo_2B-Mo_5Si_3 two-phase equilibrium as long as $\Delta G^o_{T_2} < -129$ kJ/g-atom. There are additional chemical reactions that can be used to determine the free energy of formation of T_2:

$Mo_3Si + 2MoB \leftrightarrow T_2$	$\Delta G^o_{T_2} < -126$ kJ/g-atom
$2Mo_2B + Mo_5Si_3 \leftrightarrow 2Mo + T_2$	$\Delta G^o_{T_2} < -130$ kJ/g-atom
$7T_2 + 4MoSi_2 \leftrightarrow 14MoB + 5Mo_5Si_3$	$\Delta G^o_{T_2} > -132$ kJ/g-atom

Based on these chemical reactions, bounds on the free energy of formation for T_2 were established that allowed for an estimated value of −131 ± 1 kJ/g-atom.

In a ternary system, the chemical potential of constituent element i ($i = 1$, 2, and 3) in an arbitrary α-phase, μ_i^α, is described as:[14,15]

$$\mu_1^\alpha = G^\alpha + (1 - X_1^\alpha)\left(\frac{\partial G^\alpha}{\partial X_1}\right) - X_2^\alpha\left(\frac{\partial G^\alpha}{\partial X_2}\right) \quad \text{(Eq 1a)}$$

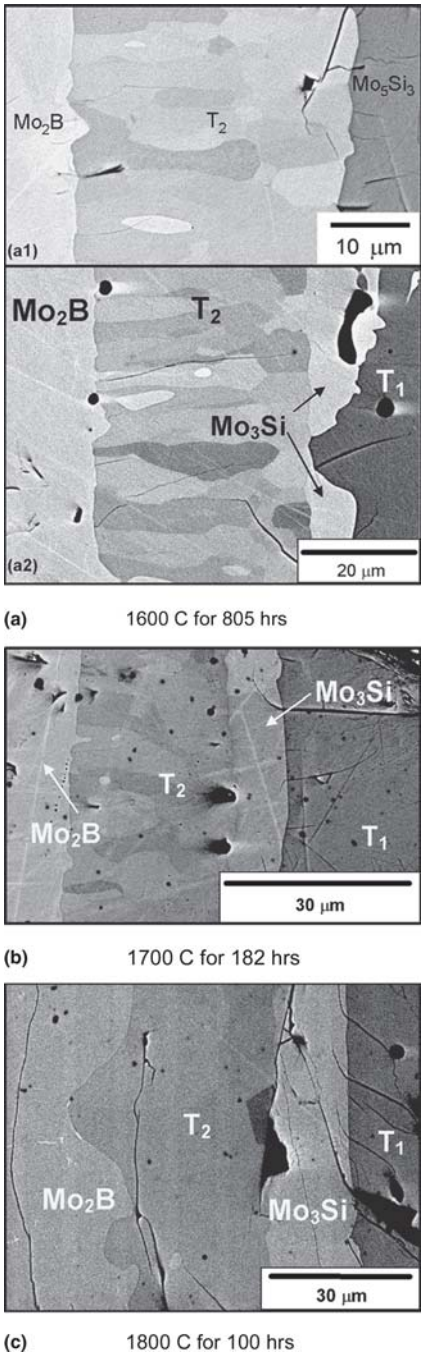

Fig. 2 BSE images of cross sections of the Mo_2B/Mo_5Si_3 diffusion couples heat-treated (a) at 1600 °C for 805 h, (b) 1700 °C for 182 h, and (c) 1800 °C for 100 h

$$\mu_2^{\alpha} = G^{\alpha} - X_1^{\alpha}\left(\frac{\partial G^{\alpha}}{\partial X_1}\right) + (1 - X_2^{\alpha})\left(\frac{\partial G^{\alpha}}{\partial X_2}\right) \quad \text{(Eq 1b)}$$

$$\mu_3^{\alpha} = G^{\alpha} - X_1^{\alpha}\left(\frac{\partial G^{\alpha}}{\partial X_1}\right) - X_2^{\alpha}\left(\frac{\partial G^{\alpha}}{\partial X_2}\right) \quad \text{(Eq 1c)}$$

$$G^{\alpha} = X_1^{\alpha}\mu_1^{\alpha} + X_2^{\alpha}\mu_2^{\alpha} + X_3^{\alpha}\mu_3^{\alpha} \quad \text{(Eq 2)}$$

where X_i is the mole fraction of i, G^{α} is the free energy of the α phase at composition $X_i = X_i^{\alpha}$, and $(\partial G^{\alpha}/\partial X_i)$ is the free-energy gradient of the α phase with respect to X_i at composition $X_i = X_i^{\alpha}$. Figure 1 shows negligible solubility of Si in Mo_2B and B in Mo_5Si_3, meaning that the free-energy gradient of Mo_2B with respect to the Si mole fraction and the free-energy gradient of Mo_5Si_3 with respect to the B mole fraction may be negligible. In this regard, Eq 1 leads to $\mu_{Si}^{Mo_2B} \approx \mu_{Mo}^{Mo_2B}$ due to $(\partial G^{Mo_2B}/\partial X_{S_i}) \approx 0$ for Mo_2B, and $\mu_B^{Mo_5Si_3} \approx \mu_{Mo}^{Mo_5Si_3}$ due to $(\partial G^{Mo_5Si_3}/\partial X_B) \approx 0$ for Mo_5Si_3. For Mo_2B, the chemical potentials of Mo and B can be determined by two common tangents between Mo_2B and Mo, and Mo_2B and MoB, so that the chemical potentials of Mo and Si can have values in a range between −118 and −103 kJ/g-atom, and the chemical potential of B can have a value in a range between −166 and −136 kJ/g-atom. From these bounds Eq 2 indicates that on a tangent plane to the Mo_2B phase free-energy surface, the free energy is −121 ± 2 kJ/g-atom at the T_2 phase stoichiometric composition. For Mo_5Si_3, the chemical potentials of Mo and Si can be determined by two common tangents between Mo_5Si_3 and Mo_3Si, and Mo_5Si_3 and $MoSi_2$, so the chemical potentials of Mo and B can have values in a range between −140 and −109 kJ/g-atom, and the chemical potential of Si can have a value in a range between −177 and −125 kJ/g-atom. Similarly, Eq 2 indicates that on a tangent plane to the Mo_5Si_3 phase free-energy surface the free energy is −128 ± 10 kJ/g-atom at the stoichiometric T_2 composition. From the estimated free energy of formation of the stoichiometric T_2 phase, the parallel tangents method[16,17] allows for an initial estimate of the driving force for nucleation of T_2 in Mo_2B at about 10 kJ/g-atom and in Mo_5Si_3 at about 3 kJ/g-atom.

For competitive phase formation the favored phase is determined by the phase with the highest nucleation rate. The nucleation rate is established mainly by the activation barrier for nucleation, ΔG^*. Since:

$$\Delta G^* \propto \sigma^3/\Delta G_N^{\ 2} \quad \text{(Eq 3)}$$

where σ is the interfacial energy between the nucleating phase and the parent structure, it is evident that the phase with the largest value of the driving force for nucleation (ΔG_N) is at an advantage to have the lowest ΔG^* value and highest nucleation rate provided the σ values for the competing phases are similar. Since detailed measurements of the relevant σ values are often not available and calculated values are normally not of high reliability, an evaluation of nucleation phase selection based on ΔG_N values can be a useful approximation when the limitations noted above are considered. Therefore, the nucleation of the T_2 phase is favored to occur in the Mo_2B phase by Si atom movements from Mo_5Si_3 to Mo_2B. Parallel with the T_2 phase nucleation on the favored Mo_2B side in the Mo_2B/Mo_5Si_3 diffusion couple, the Mo_3Si phase forms on the Mo_5Si_3 side, because Si atom movements to the Mo_2B side requires dissociation of Mo_5Si_3 into Mo_3Si and Si. Consequently, the Mo_2B/Mo_5Si_3 diffusion couple is considered to initially develop the phase sequence of $Mo_2B/T_2/Mo_3Si/Mo_5Si_3$ that agrees with the observed phase development sequence.

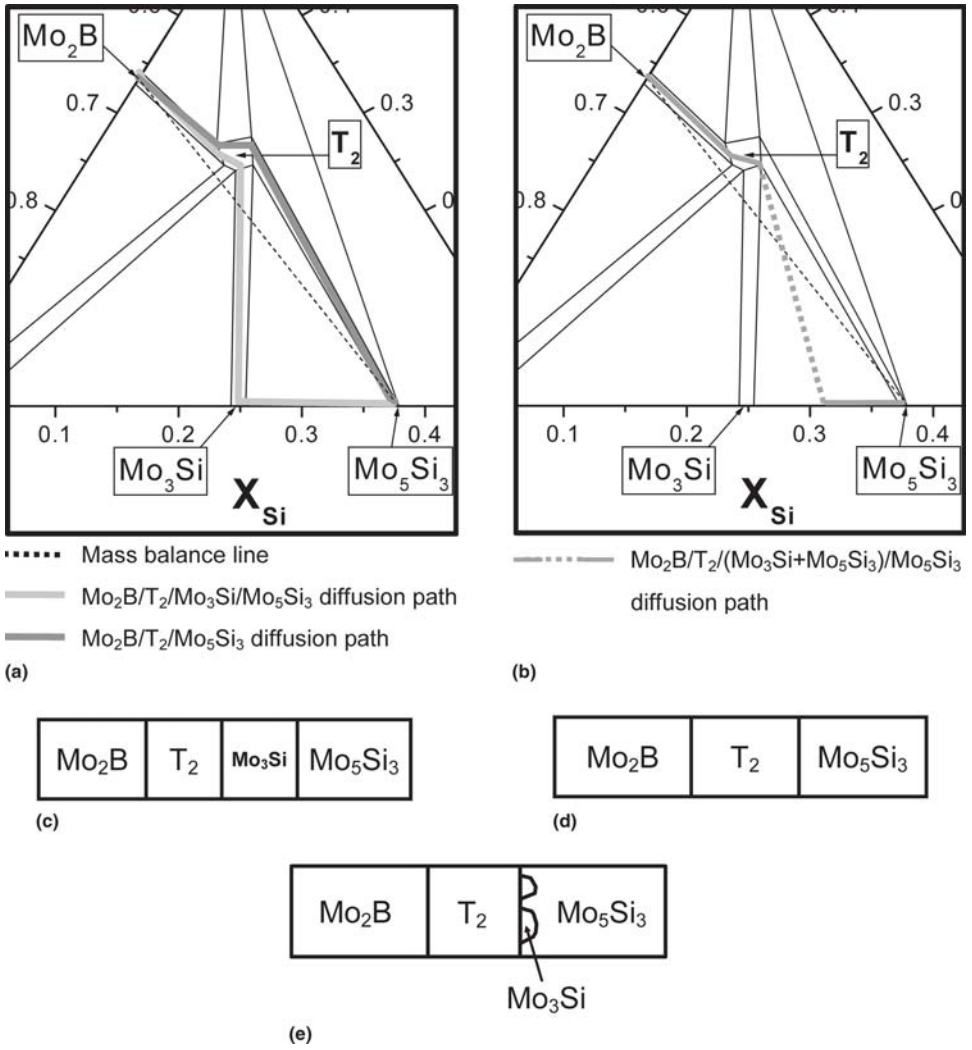

Fig. 3 Phase diagram showing (a) the $Mo_2B/T_2/Mo_3Si/Mo_5Si_3$ and $Mo_2B/T_2/Mo_5Si_3$ diffusion paths and (b) the $Mo_2B/T_2/(Mo_3Si + Mo_5Si_3)/Mo_5Si_3$ diffusion path. Schematic diagrams represent the (c) $Mo_2B/T_2/Mo_3Si/Mo_5Si_3$, (d) $Mo_2B/T_2/Mo_5Si_3$, and (e) $Mo_2B/T_2/(Mo_3Si + Mo_5Si_3)/Mo_5Si_3$ diffusion paths.

3.2 Diffusion Pathway Transition

A diffusion pathway is a representation of the relative component fluxes in a diffusion couple within a given sequence of phases. The initial sequence is established by the relative nucleation kinetics of the coexisting phases. In the Mo_2B/Mo_5Si_3 diffusion couple the initial formation of the T_2 phase in the Mo_2B layer requires Si from the Mo_5Si_3 phase. The depletion of Si results in a Mo_5Si_3 phase with a Mo supersaturation that is favorable for the nucleation and initial growth of the Mo_3Si phase. The long-term or steady-state pathway is determined by the relative magnitudes of the component fluxes between each of the phases.

Following long-term annealing at 1600 °C for 805 h in some local regions of the Mo_2B/Mo_5Si_3 diffusion couple an apparent layer sequence of $Mo_2B/T_2/Mo_5Si_3$ was observed (i.e., without Mo_3Si) as indicated in Fig. 2(a1). However, as illustrated in Fig. 3(a) this layer sequence cannot be a valid diffusion pathway since it does not satisfy mass balance. Instead, the layer arrangement in Fig. 2(a2) where the Mo_3Si phase was observed at the T_2/Mo_5Si_3 interface in other local regions is representative of the diffusion pathway (Fig. 3b). In this case, an interface formed between a single-phase (T_2) layer and a two-phase ($Mo_3Si + Mo_5Si_3$) layer. The diffusion pathways are schematically represented by the cross-section diagrams of annealed diffusion couples (Fig. 3c and d). Clark[18] noted that the interface for a single-phase layer adjacent to a two-phase layer represents an equilibrium between three phases. In this regard, long-term annealing at 1600 °C yields the $Mo_2B/T_2/(Mo_3Si + Mo_5Si_3)/Mo_5Si_3$ diffusion pathway (Fig. 3e), where a three-phase equilibrium takes place at the $T_2/(Mo_3Si + Mo_5Si_3)$ interface. A schematic diagram of the developed phase sequence in the Mo_2B/Mo_5Si_3 diffusion couple is shown in Fig. 3(e). Due to the fact that a three-phase layer cannot form in a ternary diffusion couple,[18] the $T_2 + Mo_3Si + Mo_5Si_3$ three-phase equilibrium layer is not drawn in Fig. 3(e) and a diffusion path in the $T_2 + Mo_3Si + Mo_5Si_3$

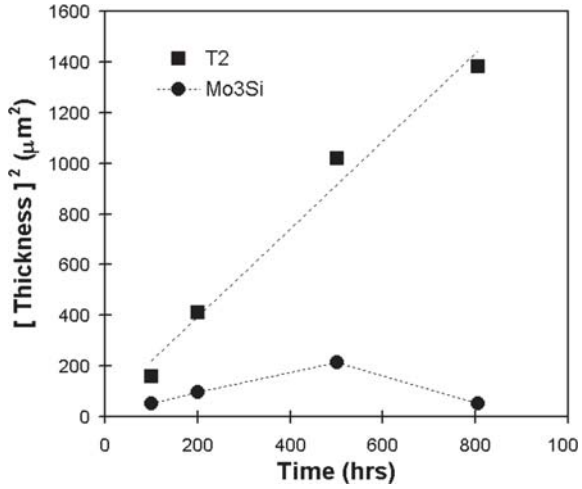

Fig. 4 Measured thickness of T_2 and Mo_3Si phases versus annealing time for a Mo_2B/Mo_5Si_3 diffusion couple annealed at 1600 °C

three-phase field is dotted in Fig. 3(b). In addition, layer growth of Mo_3Si at 1600 °C exhibits a maximum in layer growth thickness (Fig. 4), while the T_2 phase continuously grows with time. The reduction of the Mo_3Si layer thickness with extended heat treatment is further evidence that the $Mo_2B/T_2/Mo_3Si/Mo_5Si_3$ diffusion pathway is not a steady-state path, but rather reflects transient conditions (Fig. 3a).

3.3 Interdiffusion Behavior of T_2

Dayananda[19,20] developed an analysis method to determine the average interdiffusion coefficients for a phase from a single diffusion couple experiment in a multicomponent system. The average interdiffusion coefficients in a ternary system are defined as:

$$\frac{\int_{c_i^+}^{c_i^0}(x-x_0)^2dC_i}{2t(C_i^0-C_i^+)}=\overline{\tilde{D}_{ii}^n}+\overline{\tilde{D}_{ij}^n}\frac{(C_j^+-C_j^0)}{(C_i^+-C_i^0)}$$

$$\frac{\int_{c_i^0}^{c_i^-}(x-x_0)^2dC_i}{2t(C_i^--C_i^0)}=\overline{\tilde{D}_{ii}^n}+\overline{\tilde{D}_{ij}^n}\frac{(C_j^0-C_j^-)}{(C_i^0-C_i^-)} \quad \text{(Eq 4)}$$

where $(x- x_0)$ is relative distance with respect to the Matano plane at $x = x_0$, and t is annealing time. C_i^0, C_i^+, and C_i^- are concentrations of component i at $x = x_0$, $x = +\infty$, and $x = -\infty$, respectively. $\overline{\tilde{D}_{ii}^n}$ and $\overline{\tilde{D}_{ij}^n}$ are the average interdiffusion coefficients over a selected composition range of the diffusion zone. In a ternary system, Eq 4 becomes a system of two equations in two unknowns, $\overline{\tilde{D}_{ii}^n}$ and $\overline{\tilde{D}_{ij}^n}$. To have two solutions, Eq 4 should be independent, meaning that the requirements in Eq 5 should be satisfied:

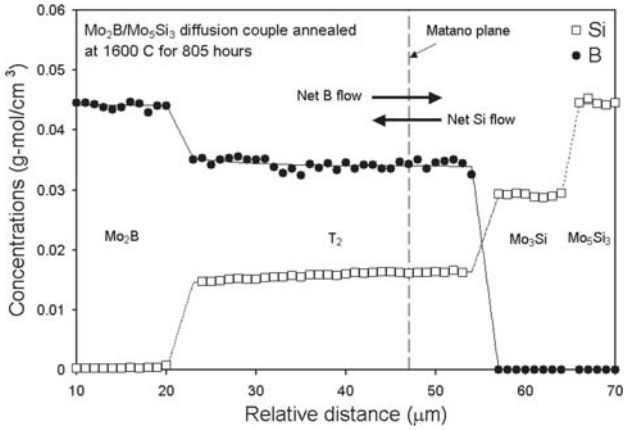

Fig. 5 Concentration profiles of Si and B obtained from EPMA measurements on the Mo_2B/Mo_5Si_3 diffusion couple annealed at 1600 °C for 805 h. Concentrations are expressed as g-atom/cm^3 through the use of molar volumes of all identified phases (7.32 cm^3/g-atom for Mo_2B, 7.70 cm^3/g-atom for T_2, 8.81 cm^3/g-atom for Mo_3Si, and 8.54 cm^3/g-atom for Mo_5Si_3). Solid and dotted smooth lines are drawn by numerically fitting a polynomial equation on concentration profile data.

$$\frac{(C_j^+-C_j^0)}{(C_i^+-C_i^0)}\neq\frac{(C_j^0-C_j^-)}{(C_i^0-C_i^-)} \text{ and } \frac{\int_{c_i^+}^{c_i^0}(x-x_0)^2dC_i}{2t(C_i^0-C_i^+)}\neq\frac{\int_{c_i^0}^{c_i^-}(x-x_0)^2dC_i}{2t(C_i^--C_i^0)} \quad \text{(Eq 5)}$$

The present diffusion couples exhibit the formation of multiple phases between terminal alloys so that the concentration profiles are not symmetric across the Matano plane. Asymmetric concentration profiles and multiple phase formation indicate that the Matano plane is not located in the middle of the T_2 phase region. In this case the diffusion profiles satisfy the above two requirements in Eq 5.

In a multicomponent system, the flux of a component depends not only on its own concentration gradient, but also on the concentration gradients of all other components in the system. In an n-component system an $(n - 1) \times (n - 1)$ square diffusivity matrix fully describes the dependence of the diffusion flux on the concentration gradients of all the components. The diffusion flux in the Mo-Si-B ternary system, therefore, depends on four independent interdiffusion coefficients, and can be expressed with the Fick's first law as:

$$\tilde{J}_{Si}=-\tilde{D}_{SiSi}^{Mo}\nabla C_{Si}-\tilde{D}_{SiB}^{Mo}\nabla C_B$$
$$\tilde{J}_B=-\tilde{D}_{BSi}^{Mo}\nabla C_{Si}-\tilde{D}_{BB}^{Mo}\nabla C_B \quad \text{(Eq 6)}$$

where $\tilde{J}_i$ is the interdiffusion flux of component i (i = Si or B), $\tilde{D}_{ij}^{Mo}$ is the interdiffusion coefficient (j = Si or B), and ∇C_j is the concentration gradient of component j. Concentration profiles of Si and B (Fig. 5) were obtained from EPMA measurements over the diffusion reaction zone between the Mo_2B and Mo_5Si_3 phases. Based on Eq 4 and the

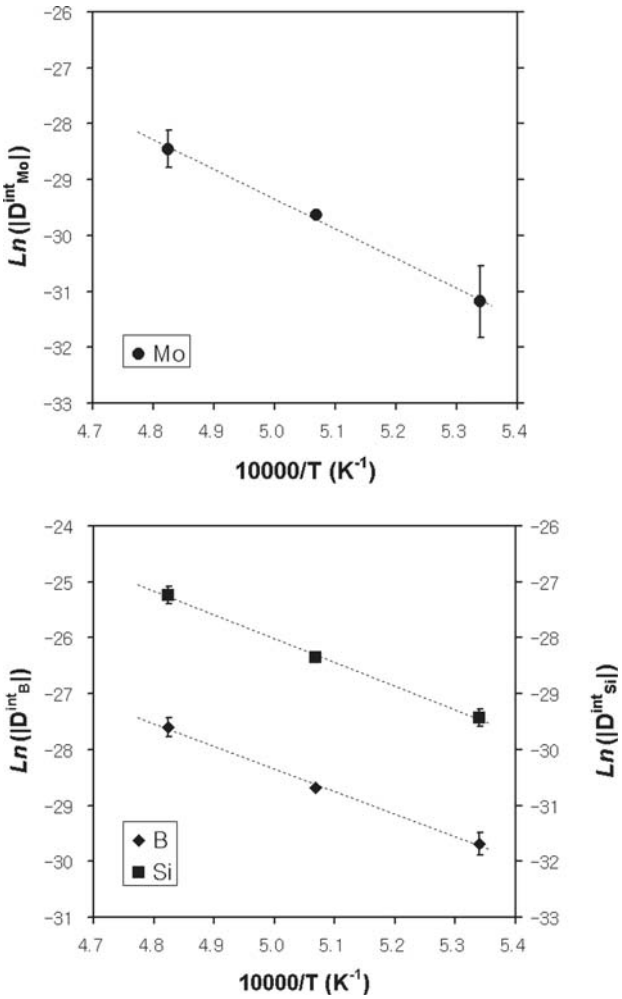

Fig. 6 Arrhenius plot of the integrated interdiffusion coefficients versus reciprocal temperature to indicate the activation energy for each $\tilde{D}_i^{int}$, (i = Mo, Si, and B). Due to negative values of $\tilde{D}_{Si}^{int}$, their absolute values were used in the plots to determine the activation energy for the i integrated interdiffusion Q_i^{int}:Q_{Mo}^{int} = 439 kJ/mol, Q_{Si}^{int} = 355 kJ/mol, and Q_B^{int} = 338 kJ/mol.

concentration profiles of Si and B, four independent average interdiffusion coefficients are estimated. The T_2 phase that developed in the Mo_2B/Mo_5Si_3 diffusion couples exhibits only small concentration changes of Si and B (≤2 at.%) elements, indicating that the interdiffusion coefficients are approximately constant. Consequently, the estimated average interdiffusion coefficients should represent closely the interdiffusion coefficients of the T_2 phase. In this regard, the interdiffusion coefficients for the T_2 phase were determined from the Mo_2B/Mo_5Si_3 diffusion couples annealed between 1600 and 1800 °C and are listed in Table 1. It is worthy to note that the estimated values of $\tilde{D}_{SiSi}^{Mo}$ and $\tilde{D}_{SiB}^{Mo}$ are positive, and $\tilde{D}_{BSi}^{Mo}$ and $\tilde{D}_{BB}^{Mo}$ exhibit negative values. Positive $\tilde{D}_{SiSi}^{Mo}$ and $\tilde{D}_{SiB}^{Mo}$ values indicate that the Si concentration gradient drives Si atoms to flow in a direction of decreasing Si concentration, while the B concentration gradient drives Si atoms to flow in an opposite direction. The Si concentration profile (Fig. 5) shows that the Si net flow occurs in the direction of negative Si concentration gradient. This indicates that the Si concentration gradient plays a key role in driving Si atom movement. Negative $\tilde{D}_{BSi}^{Mo}$ and $\tilde{D}_{BB}^{Mo}$ indicate that the Si concentration gradient drives B atoms to flow in a direction that the Si concentration increases, and the B concentration gradient drives B atoms to flow in a direction that the B concentration increases. The B concentration profile (Fig. 5) shows that B net flow occurs down the B concentration gradient. This indicates that the Si concentration gradient also plays a key role in driving B atom movement. Consequently, the Si and B diffusion behaviors reflect that Si and B atom movements in the T_2 phase are mainly controlled by the Si concentration gradient driving force.

Table 1 Interdiffusion coefficients for the T_2 phase, estimated from the Mo_2B/Mo_5Si_3 diffusion couples annealed in ranges of 1600 to 1800 °C

Temperature, °C	$\tilde{D}_{SiSi}^{Mo}$, 10^{-11} cm²/s	$\tilde{D}_{SiB}^{Mo}$, 10^{-11} cm²/s	$\tilde{D}_{BSi}^{Mo}$, 10^{-11} cm²/s	$\tilde{D}_{BB}^{Mo}$, 10^{-11} cm²/s
1600	6.1 ± 0.7	6.8 ± 0.6	−3.9 ± 0.5	−4.2 ± 0.4
1700	6.7 ± 0.6	4.4 ± 1.2	−3.5 ± 0.4	−1.8 ± 0.4
1800	62.2 ± 2.0	76.8 ± 1.4	−47.3 ± 2.9	−58.1 ± 3.1

When a compound with narrow homogeneity range develops in a diffusion couple, the concentration gradient cannot be identified so that it is impossible to determine the interdiffusion coefficient. In this regard, the integrated interdiffusion coefficient of Si, $\tilde{D}_{Si,\Delta C}^{int}$, is introduced that relates the interdiffusion coefficient to the interdiffusion flux.[19,20]

$$\tilde{D}_{Si,\Delta C}^{int} = \overline{\tilde{D}_{Si}(T_2)}\Delta C_{Si} = \int_{x_1}^{x_2} \tilde{J}_{Si}(x)\,dx \qquad \text{(Eq 7)}$$

where x_1 and x_2 are the relative distances from an arbitrary plane of reference, corresponding to boundary compositions of a T_2 phase composition range in the concentration profiles, and $\tilde{J}_{Si}(x)$ is the interdiffusion flux, ΔC_{Si} is difference between the Si concentrations at $x = x_2$ and $x = x_1$, and $\overline{\tilde{D}_{Si}(T_2)}$ represents the average effective interdiffusion coefficient of Si over the T_2 phase composition range. To compare the diffusion behavior of the T_2 phase with that observed for the Mo_5Si_3 phase, the integrated interdiffusion coefficients for the T_2 phase have been determined. Tortorici et al.[7] found the activation energy for integrated interdiffusion in $MoSi_2$ to be 130 ± 20 kJ/mol and that for Mo_5Si_3 to be 210 ± 10 kJ/mol in the Mo/Si diffusion couples annealed at 900 to 1350 °C. Their estimated integrated interdiffusion coefficient for the Mo_5Si_3 phase was 2.3 to 2.6 × 10^{-11} cm²/s at 1350 °C. Based on the integrated interdiffusion coefficients at different temperatures, the prefactor was estimated at 1.3 × 10^{-4} cm²/s so that the integrated interdiffusion coefficient at 1600 °C was evaluated to be 1.8 × 10^{-10} cm²/s. Ito et al.[10] examined the evolution kinetics of Mo_5Si_3 in the $MoSi_2$/Mo(ss) + Mo_5SiB_2 diffusion couples that were annealed in ranges of 1300 to 1500 °C. The prefactor was determined to be 1.2 ×

Table 2 Integrated interdiffusion coefficients of i (i = B, Si, Mo) for the T_2 phase in ranges of 1600 to 1800 °C and the activation energy, Q_i, for i integrated interdiffusion

	1600 °C	1700 °C	1800 °C	Q_i, kJ/mol
$\tilde{D}^{int}_{B,\Delta C}$, cm^2/s	$(1.3 \pm 0.3) \times 10^{-13}$	$(3.5 \pm 0.2) \times 10^{-13}$	$(1.0 \pm 0.2) \times 10^{-12}$	338
$\tilde{D}^{int}_{Si,\Delta C}$, cm^2/s	$(-1.7 \pm 0.1) \times 10^{-13}$	$(-4.9 \pm 0.3) \times 10^{-13}$	$(-1.5 \pm 0.2) \times 10^{-12}$	355
$\tilde{D}^{int}_{Mo,\Delta C}$, cm^2/s	$(3.5 \pm 2.0) \times 10^{-14}$	$(1.4 \pm 0.1) \times 10^{-13}$	$(4.6 \pm 1.5) \times 10^{-13}$	439

10^{-3} cm^2/s, and the activation energy for integrated interdiffusion in Mo_5Si_3 was estimated at 240 kJ/mol. The evaluated integrated interdiffusion coefficient at 1600 °C was 2.4 $\times$ 10^{-10} cm^2/s. Hayashi et al.[9] recently estimated the activation energy for integrated interdiffusion of Mo_5Si_3 in the $MoSi_2/T_2$ diffusion couple at about 300 kJ/mol, and the integrated interdiffusion coefficient for Mo_5Si_3 was 3.1 $\times$ 10^{-10} cm^2/s at 1600 °C. The estimated interdiffusion coefficients for the T_2 phase in the current study are listed in Table 2, in which the integrated interdiffusion coefficients of B, Si, and Mo at 1600 °C are 1.3×10^{-13} cm^2/s, -1.7×10^{-13} cm^2/s, and 3.5×10^{-14} cm^2/s, respectively (Fig. 6). The activation energies for Mo, Si, and B integrated interdiffusions are 439, 355, and 338 kJ/mol, respectively. Table 2 reveals that the integrated interdiffusion coefficient of Si in the T_2 phase is smaller by about three orders of magnitude than that for the Mo_5Si_3 phase. The activation energies for integrated interdiffusion of Si for the T_2 phase is 355 kJ/mol, that is, larger by 56 kJ/mol than that[9] for the Mo_5Si_3 phase. The 10^3 difference between the integrated interdiffusion coefficients of Si for the T_2 and Mo_5Si_3 phases appears to mainly originate from differences in the activation energy because $\exp(-\Delta Q/RT) = 2.7 \times 10^{-2}$ at 1600 °C.

Another factor for the difference in the integrated interdiffusion coefficient can be identified in the correlation effect that is related to the atomic jump process by a vacancy mechanism. In general, successive jumps of an atom by the vacancy mechanism tend to have displacements in opposite directions, meaning that an atom having exchanged with a vacancy has a better than random chance of the reverse jump. The correlation effect depends significantly on the crystal structure and the anisotropic jump frequency. The SEM-BSE images in Fig. 2 show that microstructure of the T_2 phase is columnar. A TEM analysis[11] revealed that the T_2 phase synthesized in the Mo_2B/Mo_5Si_3 diffusion couple grows perpendicular to the tetragonal axis. The tetragonal T_2 phase, as shown in Fig. 7, also reveals the highly ordered $D8_l$ structure, consisting of three different types of layers:[21,22] Mo layer (A layer), Mo + B layer (B layer), and Si layer (C layer). The T_2 structure is constructed in a stacking arrangement involving successive layers of:

$$\ldots BACA_{1/21/2}BA_{1/21/2}CABACA_{1/21/2}BA_{1/21/2}CA \ldots$$

along the tetragonal axis, where the $A_{1/21/2}$ layer refers to the A layer that has been translated by half the base diagonal relative to neighboring layers. This indicates that atom diffusion in the T_2 phase occurs perpendicular to the tetragonal axis and along the layer plane, meaning that diffusion in the T_2 phase is highly anisotropic. For the anisotropic $MoSi_2$ phase Salamon et al.[23] and Divinski et al.[24] reported Si and Mo diffuse independently on their own sublattices. In addition, the anisotropy ratio ($D_\perp/D_\parallel$) of the self-diffusion coefficients perpendicular ($\perp$) and parallel ($\parallel$), respectively, to the tetragonal axis varied between 10 and 100. The reduced correlation factor in a crystal structure revealing the anisotropic diffusion behavior can also contribute to a low diffusivity for the T_2 phase.

A closer inspection of the structure of Mo_5Si_3 in Fig. 7 reveals both Mo and Si sublattice sites, where an atom occupying the Mo sublattice site in Mo_5Si_3 is surrounded by Mo and/or Si species atoms, and an atom on the Si sublattice site is surrounded by Mo and/or Si species atoms. However, the T_2 phase is constructed by four different Mo_I, Mo_{II}, Si, and B sublattice sites.[21] Whenever an atom substitutionally jumps to an adjacent site, it is surrounded by one of four different configurations of Mo, Si, and B atoms and vacancies that limit the jump options. Moreover, based on the lattice parameters of T_2 ($a = 0.601$ nm and $c = 1.103$ nm) and Mo_5Si_3 ($a = 0.962$ nm and $c = 0.49$ nm), the packing efficiency was determined to be 67% for the T_2 phase and 63% for the Mo_5Si_3 phase. As a result, an atom or vacancy in the T_2 phase is surrounded by more complex and denser-packed neighboring configurations than in the Mo_5Si_3 phase, but the influence of these conditions on the diffusion behavior requires further analysis.

The relatively slow diffusion in the T_2 phase is also consistent with the superior high-temperature creep resistance of T_2 phase based microstructures. For example, activation energies estimated from creep tests at similar flow stress levels were reported to be 399 kJ/mol for the Mo_5Si_3 phase,[25,26] and 415 to 445 kJ/mol for the Mo(ss) + T_2 two-phase alloys.[27] The creep rate of a multicomponent alloy is proportional to the interdiffusion coefficient:[25,28] $\dot{\varepsilon} \propto \tilde{D}\sigma^n$, where $\dot{\varepsilon}$ is the creep rate, $\tilde{D}$ is the interdiffusion coefficient, σ is the applied creep stress, and n is the creep stress exponent. As long as the applied creep stress is constant, the creep strain rate is dependent on the interdiffusion coefficient. A high activation energy for interdiffusion decreases the interdiffusion coefficient that subsequently decreases the creep rate.

4. Summary

Diffusion couples consisting of binary boride and silicide phases have been used to determine the diffusion kinetics of T_2 phase development. Following diffusion anneals between 1600 and 1800 °C an initial diffusion pathway sequence of $Mo_2B/T_2/Mo_3Si/Mo_5Si_3$ developed, which was

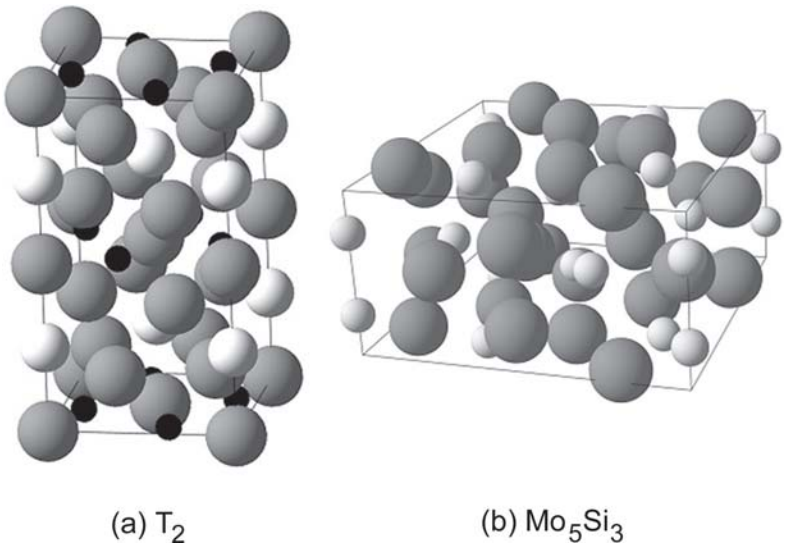

Fig. 7 Crystal structure of the (a) T_2 and (b) Mo_5Si_3 phases, in which a gray sphere represents Mo atom, a white sphere represents Si atom and a black sphere represents B atom. Based on the lattice parameters (for T_2: $a = 0.601$ nm and $c = 1.103$ nm; for Mo_5Si_3: $a = 0.962$ nm and $c = 0.49$ nm), the packing efficiency was determined to be 67% for the T_2 phase and 63% for the Mo_5Si_3 phase.

subsequently transformed to $Mo_2B/T_2/(Mo_3Si + Mo_5Si_3)/Mo_5Si_3$ by shrinkage of the Mo_3Si phase on long-term annealing. During the growth of T_2, Si, and B atom movements were driven by the Si concentration gradient. The measured integrated interdiffusion coefficients at 1600 °C in the T_2 phase are 1.3×10^{-13} cm^2/s, -1.7×10^{-13} cm^2/s, and 3.5×10^{-14} cm^2/s for B, Si, and Mo, respectively. The 10^3 smaller integrated interdiffusion coefficient for Si in T_2 compared with Mo_5Si_3 is mainly due to the larger activation energy for Si diffusion, but the observed anisotropic growth of the T_2 phase product layer also suggests a relatively small correlation coefficient.

Acknowledgments

The support of the AFOSR (FA9550-06-1-0233) is gratefully acknowledged. The authors would like to thank Dr. J. Fournelle for expert guidance with EPMA measurements. The authors appreciate valuable discussions with Professor Y.-H. Sohn of the University of Central Florida and Professor M. Dayananda of Purdue University and constructive guidance from the referee.

References

1. S. Kim and J. H. Perepezko, to be published
2. K. Ito, K. Ihara, K. Tanaka, M. Fujikura, and M. Yamaguchi, Physical and Mechanical Properties of Single Crystals of the T_2 Phase in the Mo-Si-B System, *Intermetallics,* 2001, **9,** p 591-602
3. F. Christian, H. Sohma, T. Tanaka, H. Tanaka, K. Ohsasa, and T. Narita, Growth Rate Constant and Chemical Diffusivity in Silicides Mo_5Si_3 and Ta_5Si_3, *Mater. Trans. JIM,* 1998, **39,** p 286-291
4. R.W. Bartlett, P.R. Gage, and P.A. Larssen, Growth Kinetics of Intermediate Silicides in the $MoSi_2$/Mo and WSi_2/W Systems, *Trans. TMS-AIME,* 1964, **230,** p 1528-1534
5. E. Fitzer and K. Matthias, On Silicon Diffusion in the Tetragonal and the Carbon-Stabilized Hexagonal Mo_5Si_3 Phase, *High Temp. Sci.,* 1971, **3,** p 93-98
6. R.W. Bartlett, Kinetics of Ta_5Si_3 and Cb_5Si_3 Growth of Disilicide Coatings on Tantalum and Columbium, *Trans. TMS-AIME,* 1966, **236,** p 1230-1231
7. P.C. Tortorici and M.A. Dayananda, Growth of Silicides and Interdiffusion in the Mo-Si System, *Metall. Mater. Trans. A,* 1999, **30A,** p 545-550
8. J. Brandstötter and W. Lengauer, Multiphase Reaction Diffusion in Transition Metal-Boron Systems, *J. Alloy. Compd.,* 1997, **262-263,** p 390-396
9. T. Hayashi, K. Ito, and H. Numakura, Reaction Diffusion of $MoSi_2$ and Mo_5SiB_2, *Intermetallics,* 2005, **13,** p 93-100
10. K. Ito, T. Hayashi, M. Yokobayashi, and H. Numakura, Evolution Kinetics and Microstructure of $MoSi_2$ and Mo_5Si_3 Surface Layers on Two-phase Mo-9Si-18B Alloy During Pack-cementation and High-temperature Oxidation, *Intermetallics,* 2004, **12,** p 407-415
11. S. Kim, R. Sakidja, Z. Dong, J.H. Perepezko, and Y.W. Kim, Growth of the Mo_5SiB_2 Phase in a Mo_5Si_3/Mo_2B Diffusion Couple, *Mater. Res. Soc. Symp. Proc.,* 2001, **646**, p N5.42.1-N5.42.6
12. J.H. Fournelle, J.J. Donovan, S. Kim, and J.H. Perepezko, Analysis of Boron by EPMA: Correction for Dual Mo and Si Interferences for Phases in the Mo-Si-B System, *Inst. Phys. Conf. Ser.,* 2000, **No. 165**, p 425-426
13. O. Kubaschewski, C.B. Alcock, and P.J. Spencer, *Materials Thermochemistry,* 6th ed., Pergamon Press, New York, 1993, p 257-323
14. D.R. Gaskel, *Introduction to Metallurgical Thermodynamics,* 2nd ed., McGraw-Hill, New York, 1981
15. C.H.P. Lupis, *Chemical Thermodynamics of Materials,* Elsevier Science, New York, 1983
16. C.V. Thompson and F. Spaepen, Homogeneous Crystal Nucleation in Binary Metallic Melts, *Acta Metall.,* 1983, **31,** p 2021-2027
17. J.W. Christian, *The Theory of Transformations in Metals and*

Alloys, 1st ed., Pergamon Press, Oxford, UK, 1965, p 537-541

18. J.B. Clark, Conventions for Plotting the Diffusion Paths in Multiphase Ternary Diffusion Couples on the Isothermal Section of a Ternary Phase Diagram, *TMS-AIME,* 1963, **227,** p 1250-1251
19. M.A. Dayananda, Average Effective Interdiffusion Coefficients and the Matano Plane Composition, *Metall. Mater. Trans. A,* 1996, **27A,** p 2504-2509
20. M.A. Dayananda and Y.H. Sohn, A New Analysis for the Determination of Ternary Interdiffusion Coefficients from a Single Diffusion Couple, *Metall. Mater. Trans. A,* 1999, **30A,** p 535-543
21. B. Aronsson, The Crystal Structure of Mo_5SiB_2, *Acta Chem. Scand. A,* 1958, **12,** p 31-37
22. C.J. Rawn, J.H. Schneibel, C.M. Hoffmann, and C.R. Hubbard, The Crystal Structure and Thermal Expansion of Mo_5SiB_2, *Intermetallics,* 2001, **9,** p 209-216
23. M. Salamon, A. Strohm, T. Voss, P. Laitinen, I. Riihimäki, S. Divinski, W. Frank, J. Räisänen, and H. Mehrer, Self-Diffusion of Silicon in Molybdenum Disilicide, *Philos. Mag.,* 2004, **84,** p 737-756
24. S. Divinski, M. Salamon, and H. Mehrer, Silicon Diffusion in Molybdenum Disilicide: Correlation Effects, *Philos. Mag.,* 2004, **84,** p 757-772
25. M.K. Meyer, M.J. Kramer, and M. Akinca, Compressive Creep Behavior of Mo_5Si_3 with the Addition of Boron, *Intermetallics,* 1996, **4,** p 273-281
26. M. Akinc, M.K. Meyer, M.J. Kramer, A.J. Thom, J.J. Huebsch, and B. Cook, Boron-Doped Molybdenum Silicides for Structural Applications, *Mater. Sci. Eng. A,* 1999, **A261,** p 16-23
27. A.P. Alur, N. Chollacoop, and K.S. Kumar, High-Temperature Compression Behavior of Mo-Si-B Alloys, *Acta Mater.,* 2004, **52,** p 5571-5587
28. K.L. Murty, F.A. Mohamed, and J.E. Dorn, Viscous Glide, Dislocation Climb and Newtonian Viscous Deformation Mechanisms of High Temperature Creep in Al-3Mg, *Acta Metall.,* 1972, **20,** p 1009-1018